kapteyn astronomical
institute

Observing the Sun with KISS

Petar I. Penchev, S4683099, p.i.penchev@student.rug.nl

Abstract: This study investigates the angular size and structure of the radio Sun using the Kapteyn Interferometer for Short-baseline Solar observations (KISS). By analyzing visibility patterns at different baselines, we estimate the Sun's radio diameter and its shape. Our results indicate that the Sinc function provides the best fit, suggesting a square-like shape. Despite having limited baseline data, our findings demonstrate the effectiveness of short-baseline interferometry in solar observations.

1 Introduction

Radio interferometry started back in 1946 with its inventors being Martin Ryle and Tony Hewish. By using two radio telescopes and changing the distance between them, Sir Martin Ryle showed that you can increase the resolution of observation. This telescope system was used in the discovery of the first pulsar in 1967 by Hewish and Jocelyn Bell. For their achievements both Ryle and Hewish jointly received the Nobel Prize in Physics in 1974.

One of the first working interferometers to be used for astronomical observations was the Sea Cliff Interferometer, also invented back in 1946 by Joseph Lade Pawsey. It relied on reflections from the sea to do the interferometry. The first model was located at Dover Heights in Australia [Wild (1987)].

In this project we are trying to measure the size and shape of the radio Sun using the Kapteyn Interferometer for Short-baseline Solar observations (KISS). The telescope was build by Mathijn Lensen (frontend), Casper F. Jentink (backend), and Jasper Steringa (simulations). More about the telescope in Section 3.

2 Theory

2.1 Interferometry

Interferometry is a technique which uses two (or more) filled aperture to create a bigger unfilled aperture by superimposing the responses of each aperture. This way we can increase the angular resolution of our observation. For a single dish this is proportional to,

$$\theta \propto \frac{\lambda}{D}, \tag{2.1}$$

where D is the diameter of our dish. For an interferometer this equation becomes,

$$\theta \propto \frac{\lambda}{B}, \tag{2.2}$$

where B is the baseline of the interferometer, defined as the distance between the two filled apertures. As we can see the angular resolution is inversly proportional to the baseline, meaning that a bigger baseline gives us better angular resolution (the best in astronomy).

Given the fact that the two responses are usually out of phase due to the geometric delay between the two dishes, the response of an interferometer is a interference pattern across the field-of-view (FOV). A schematic representation of a simple setup can be seen in the figure bellow.

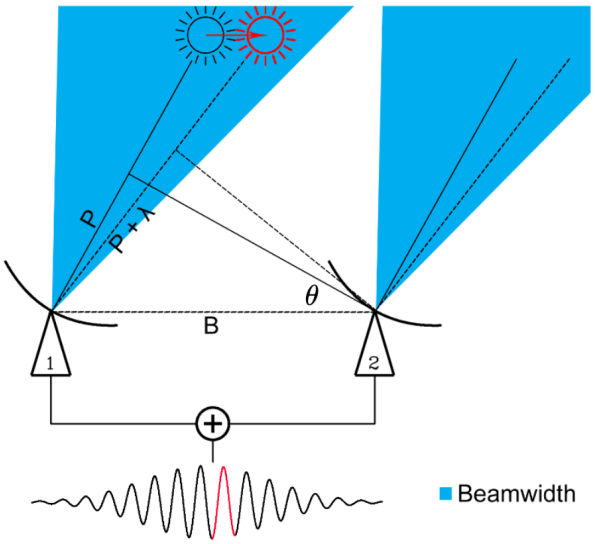

Figure 2.1: A schematic representation of two element interferometer, where B represents the baseline and P the geometric delay.

2.2 Fringe Visibility

Visibility is defined as the ratio of the amplitude of the interference pattern to the sum of the powers of the individual waves. The interferometric visibility gives a practical way to measure the coherence of two waves (or one wave with itself).

In the case of interferometer, two waves are superimposed, due to the contribution from each dish to the power. This forms an interference pattern. The power peaks when the sun is at the (HPBW) of the interferometer, and since the sun is in the far field we have a Gaussian like pattern of the Delay Beam. For the Young's double slit experiment this looks something like in the figure bellow.

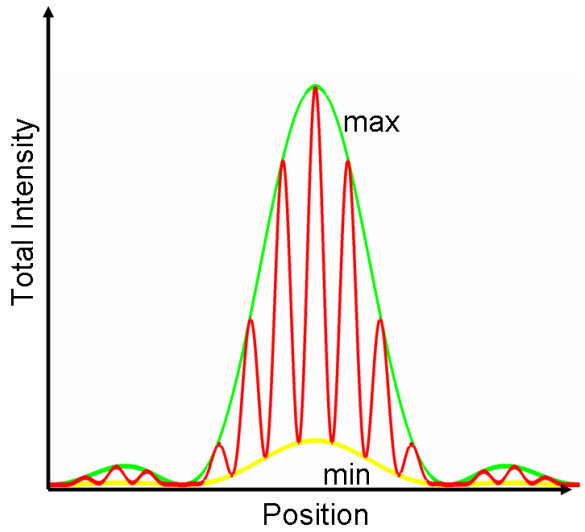

Figure 2.2: The figure represents the visibility of the double-slit interference.

The visibility can be modeled by taking the amplitude of the maximum and minimum power, modeled by a Gaussians, and relating them in the following way,

$$|V(B_\lambda)| = \frac{P_{max} - P_{min}}{P_{max} + P_{min}}, \tag{2.3}$$

where P_{max} is the amplitude of the big Gaussian (the green line in Figure 2.2), and P_{min} is the amplitude of the small Gaussian (the red line in Figure 2.2).

2.3 Power Average

In order to get our synthesized beam and get a better idea of how the fringe visibility is related to our baseline we need to substract the average power from our data. The average power can be defined using the Gaussian trick as described above as,

$$P_{avg}(t) = \frac{P_{max}(t) + P_{min}(t)}{2}, \tag{2.4}$$

where $P_{max}(t)$ and $P_{min}(t)$ is the value of the big and small Gaussian respectively at time t. This means that our synthesized beam is given by,

$$Synthesized\ Beam = Data - P_{avg}. \tag{2.5}$$

2.4 Baseline Determination

Since we know that the Full-width half maximum (FWHM) of a single dish is given by,

$$\theta_{FWHM} = \frac{\lambda}{D}, \tag{2.6}$$

we can rewrite our fringe width as,

$$W_{fringe} = \frac{\theta_{FWHM} D}{B} \tag{2.7}$$

where D is the diameter of the dish and B is the baseline. Thus if we solve for the baseline we have that,

$$B_\lambda = \frac{\theta_{FWHM} D}{\lambda W_{fringe}}. \tag{2.8}$$

2.5 Determining the shape of the radio Sun

The response of an interferometer is the (inverse) Fourier transform of the sky brightness distribution. To infer the true surface brightness distribution of an object, such as the radio Sun, we analyze the visibility as a function of baseline. This approach avoids the need for complete sampling of the uv-plane, which is often impractical.

In our analysis, we fit mathematical models such as sinc functions and Bessel functions to the observed visibility data. These functions correspond to idealized brightness distributions in the sky.

The first root in these visibility functions provides an estimate of the angular size of the object. Deviations from the models can indicate the presence of more complex structures, such as sunspots or extended regions such as solar arcs. These deviations would not be explored in this report due to the limitations of the instrument.

Sinc function

A sinc function is associated with a uniformly bright square, representing a simple model of the Sun's radio emission. It is given by the following equation,

$$V(B_\lambda) = a\text{sinc}(bB_\lambda) \tag{2.9}$$

Here is a figure representing the modeled sinc fit.

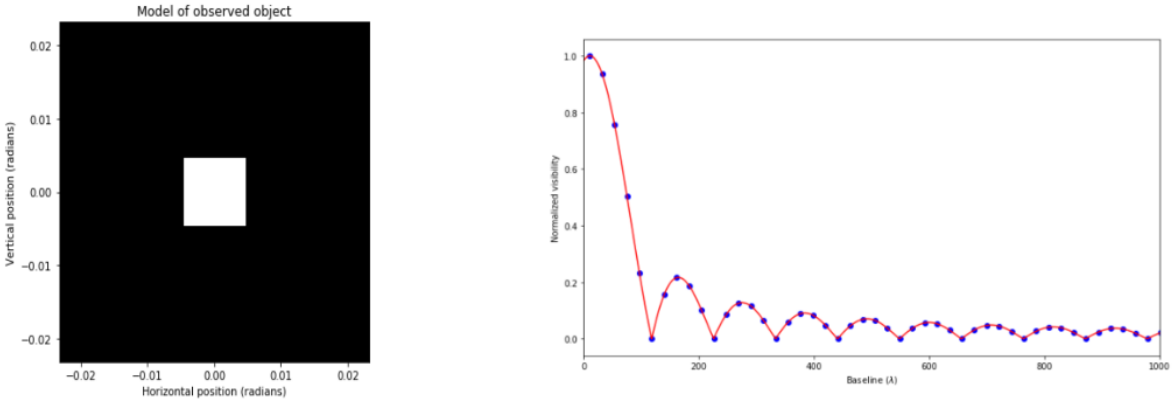

Figure 2.3: A modeled sinc function fit.

Bessel function

A Bessel function can describe more realistic cases, such as the emission from a partially resolved disk or structures with radial symmetry. It is described using the following equation,

$$V(B_\lambda) = 2\pi ab\frac{J_1(aB_\lambda)}{B_\lambda}. \tag{2.10}$$

Here is a figure representing the modeled Bessel fit.

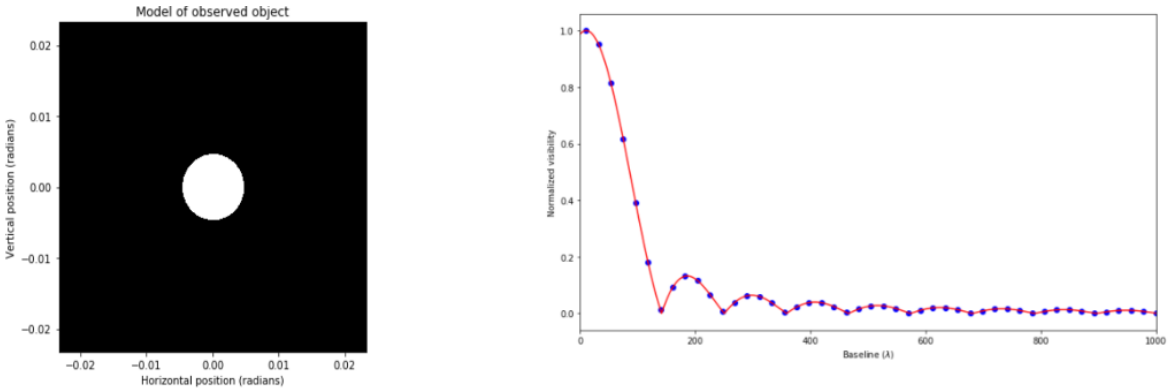

Figure 2.4: A modeled Bessel function fit.

Bessel Donnut function

A Bessel Donnut function in the context of this report is referred to as a punctured disk. It is described by the difference of two Bessel functions with the one with a smaller angular size substracted from the bigger one. It is given by the following equation,

$$V(B_\lambda) = V_{large\ disk} - V_{small\ disk}. \tag{2.11}$$

Here is a figure representing the modeled Bessel Donnut fit.

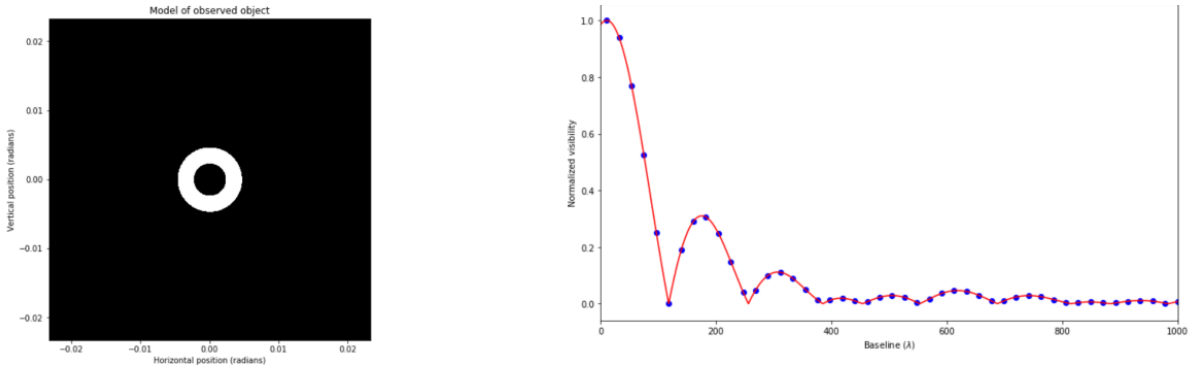

Figure 2.5: A modeled Bessel Donnut function fit.

3 Observations

Kapteyn Interferometer for Short-baseline Solar observations (KISS)

The instrument we are using is equipped with two dishes, each with a diameter of $D = 0.35\,\mathrm{m}$. The interferometer is sensitive to frequencies in the range $\nu = 11.21 - 11.29\,\mathrm{GHz}$. The telescope has a half-power beam width (HPBW) of $\theta_{\mathrm{HPBW}} = 4.9°$. The separation between the two dishes, also known as the baseline, is varied for each dataset, with a total of eight different baselines used in each dataset.

These eight measurements were conducted between May 9 and June 6, 2018. Each observation is accompanied by notes highlighting events deemed important by the observation team. For more details, refer to the thesis of Casper Farret Jentink [Jentink (2018)].

Notable Events

Two notes from Jentink's notebook are particularly noteworthy. The first reports a person standing in front of one of the dishes on the third day of observation. The second refers to the seventh day of observation when the team experimented with the shortest baseline.

The remaining observations appear to have been conducted under good conditions, without notable disruptions.

4 Results

4.1 Preprocessing the data

We start by examining the raw data. The raw data consists of the power measured by the KISS radiometer in terms of the time of observation. A figure of the data can be seen below.

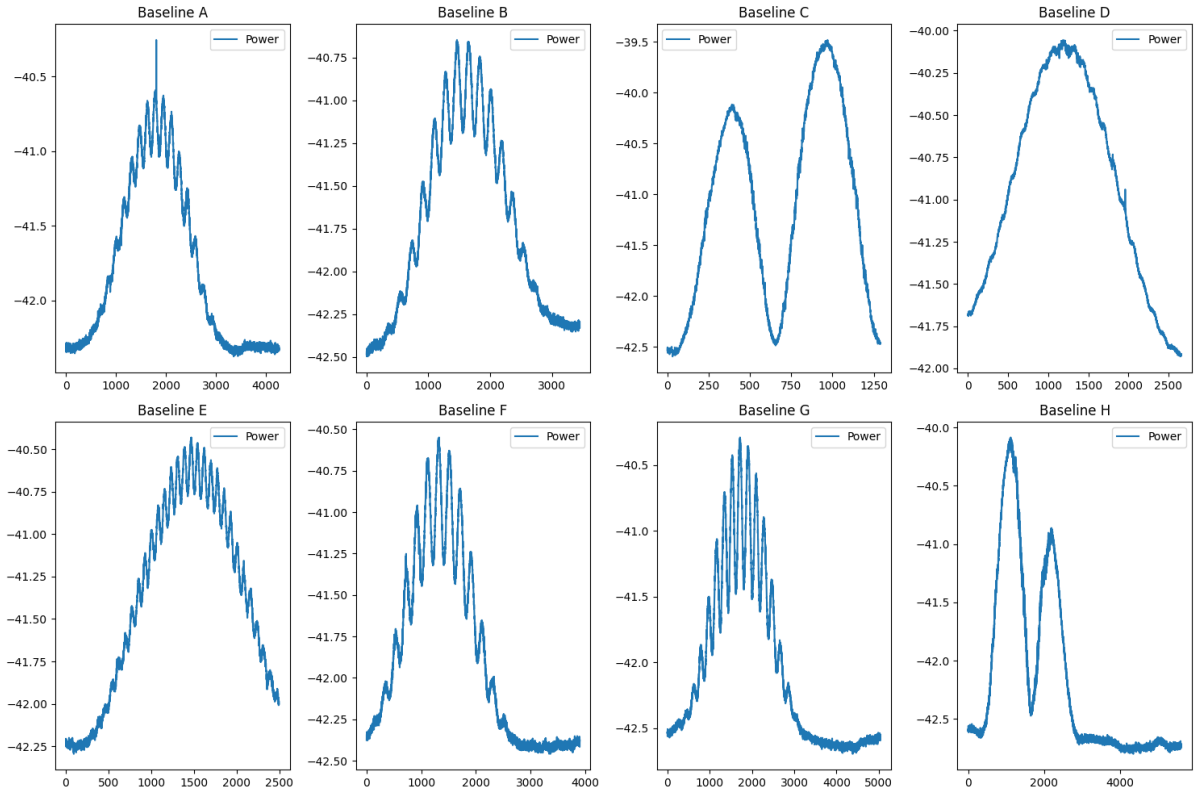

Figure 4.1: The raw data as taken by the KISS radiometer. The y-axis is the power as measured in dBm while the x-axis is the time as measured in seconds.

We first need to convert the power from dBm to Watts. We do that using the following releation,

$$P[W] = 10^{-3} W 10^{(P[dBm]/10)}, \tag{4.1}$$

where the symbols have their usual meaning. After that we need to find the peaks and the troughs of the synthesized beam. This is done using the $find\_peaks$ function from the *scipy.signal* module [Developers (2025b)]. After we are done we use the $curve\_fit$ function from the *scipy.optimize* module [Developers (2025a)] to fit Gaussians through the peaks and the troughs. The result of this fit can be seen below.

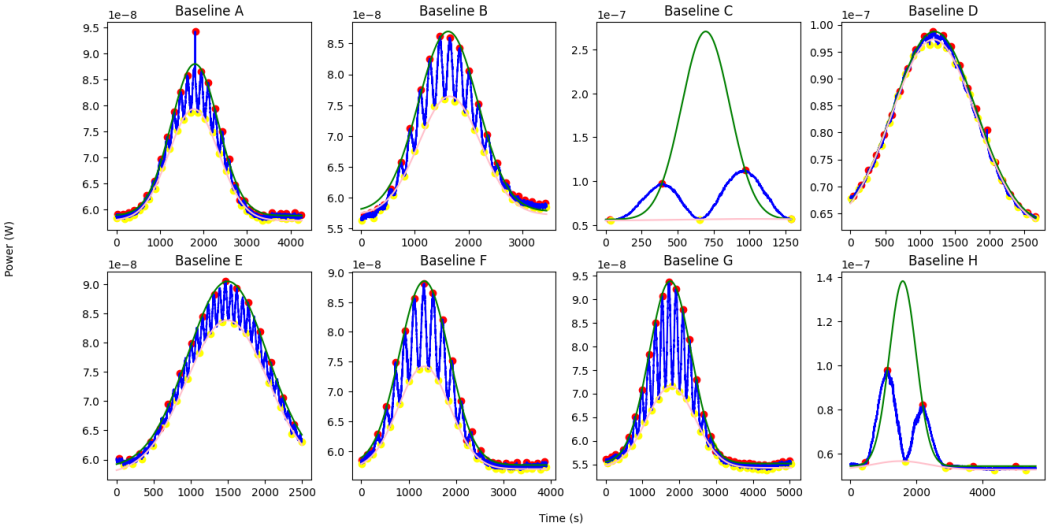

Figure 4.2: The figure shows the fitted Gaussians through the peaks and troughs of the synthesized beam for each of the 8 baselines. The peak at around $9.5 \times 10^{-8} W$ in baseline A is ignored as it is clear that it is just an outlier.

After we have fitted the Gaussians we can now demean the data by applying Equation 2.5. It is useful to convert the time to degrees. Considering the fact that it takes 24 hours for the earth to revolve once on its axis, and that the celestial sphere has 360° we can use simple algebra and convert time to degrees using,

$$deg[\circ] = \frac{t[s] \times 360^\circ}{24h \times 60m \times 60s}, \tag{4.2}$$

which basically tells us how many degrees in the sky the sun moves during our observation. After this transformation we can now get the normalized beam.

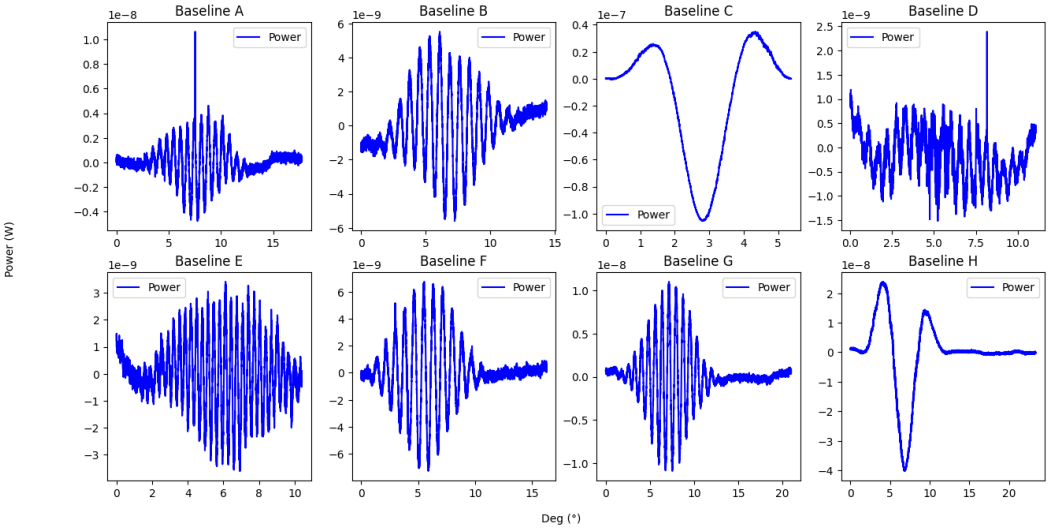

Figure 4.3: The figure shows the demeaned synthesized beam pattern of our interferometer for each baseline.

Finding the baselines

After all the preprocessing we can now proceed with finding the width of the fringes. First we need to narrow down to the fringes corresponding roughly to the HPBW of the instrument. After isolating two adjacent peaks we can perform the seam peak search like we did in the previous section to find the width of the fringes. This can be seen in the figure below.

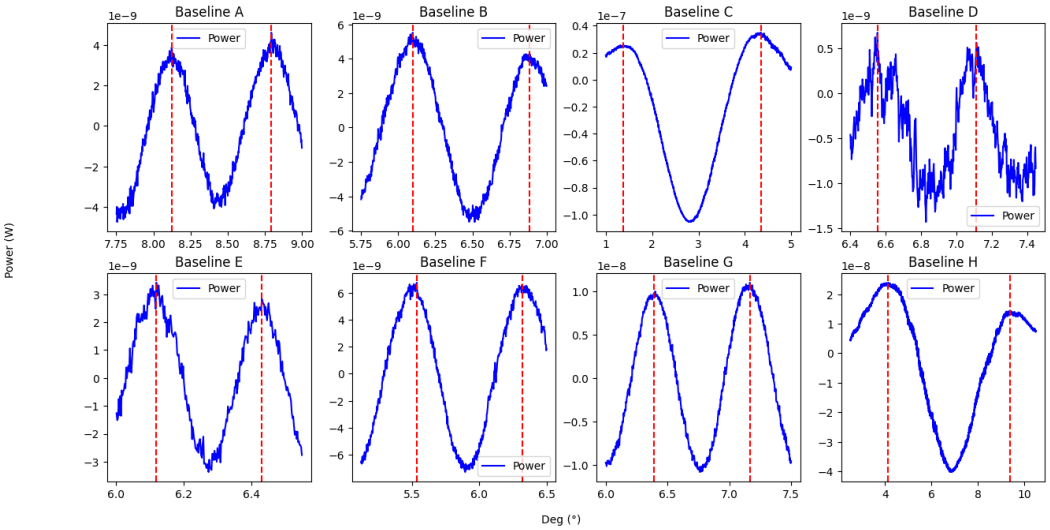

Figure 4.4: The figure shows two peasks, approximately at the HPBW of each baseline. The red dashed lines represent the peaks and hence the space between them is our fringe width.

Finding the fringe width is a straight forward procedure, we take the absolute value of the difference between two adjacent peaks and convert it from degrees to radiance. The summary of the W_{fringe} results can be seen in the table below.

Baseline	W_{fringe} **(rad)**
Baseline A	0.012
Baseline B	0.014
Baseline C	0.052
Baseline D	0.010
Baseline E	0.005
Baseline F	0.014
Baseline G	0.014
Baseline H	0.092

Table 4.1: Fringe width values in radians.

Using Equation 2.8 we can compute the baseline for each of the dataset, the results of which can be seen in the table below.

Baseline	A	B	C	D	E	F	G	H
Value	85.439	72.722	19.266	102.477	183.926	73.299	73.991	10.885

Table 4.2: Baseline values.

Finding the visibilities

We can use the Gaussian fit that we did earlier (refer to Figure 4.4) to compute the visibilites for each dataset. We know that the visibility is dependent on the amplitudes of said Gaussians through the relation

described by Equation 2.3. We can find the P_{max} and P_{min} by summing the offset to the amplitudes of each gaussian,

$$P_{max} = A_{big} + offset_{big} \tag{4.3}$$

$$P_{min} = A_{small} + offset_{small} \tag{4.4}$$

After we have found these we can compute the visiblities of each dataset which can be found, along with the values for P_{max} and P_{min} in the table below (refer to Appendix B for error propagation)

Baseline	Power (W)	Visibility
A	$P_{\max} = 8.801 \times 10^{-8} \pm 1.553 \times 10^{-19}$ $P_{\min} = 7.933 \times 10^{-8} \pm 4.757 \times 10^{-20}$	$\lvert V(B_\lambda)\rvert = 0.052 \pm 9.292 \times 10^{-13}$
B	$P_{\max} = 8.696 \times 10^{-8} \pm 3.359 \times 10^{-19}$ $P_{\min} = 7.643 \times 10^{-8} \pm 2.372 \times 10^{-19}$	$\lvert V(B_\lambda)\rvert = 0.064 \pm 2.467 \times 10^{-12}$
C	$P_{\max} = 2.708 \times 10^{-7} \pm \infty$ $P_{\min} = 5.683 \times 10^{-8} \pm \infty$	$\lvert V(B_\lambda)\rvert = 0.653 \pm \infty$
D	$P_{\max} = 9.872 \times 10^{-8} \pm 4.699 \times 10^{-19}$ $P_{\min} = 9.727 \times 10^{-8} \pm 5.312 \times 10^{-19}$	$\lvert V(B_\lambda)\rvert = 0.007 \pm 3.622 \times 10^{-12}$
E	$P_{\max} = 9.053 \times 10^{-8} \pm 3.010 \times 10^{-19}$ $P_{\min} = 8.387 \times 10^{-8} \pm 1.874 \times 10^{-19}$	$\lvert V(B_\lambda)\rvert = 0.038 \pm 2.000 \times 10^{-12}$
F	$P_{\max} = 8.854 \times 10^{-8} \pm 2.976 \times 10^{-19}$ $P_{\min} = 7.421 \times 10^{-8} \pm 1.865 \times 10^{-20}$	$\lvert V(B_\lambda)\rvert = 0.088 \pm 1.672 \times 10^{-12}$
G	$P_{\max} = 9.379 \times 10^{-8} \pm 7.024 \times 10^{-20}$ $P_{\min} = 7.149 \times 10^{-8} \pm 6.101 \times 10^{-20}$	$\lvert V(B_\lambda)\rvert = 0.135 \pm 5.574 \times 10^{-13}$
H	$P_{\max} = 1.383 \times 10^{-7} \pm 7.340 \times 10^{-19}$ $P_{\min} = 5.660 \times 10^{-8} \pm 2.497 \times 10^{-19}$	$\lvert V(B_\lambda)\rvert = 0.419 \pm 2.844 \times 10^{-12}$

Table 4.3: Power and Visibility Data for Different Baselines. The ∞ error in Baseline C is due to numerical instability in computing the covariance matrix of the fit.

Fitting the functions

Now that we have the visibility for each baseline we can try and fit the functions described in Section 2.5. The fits can be seen in the figure below.

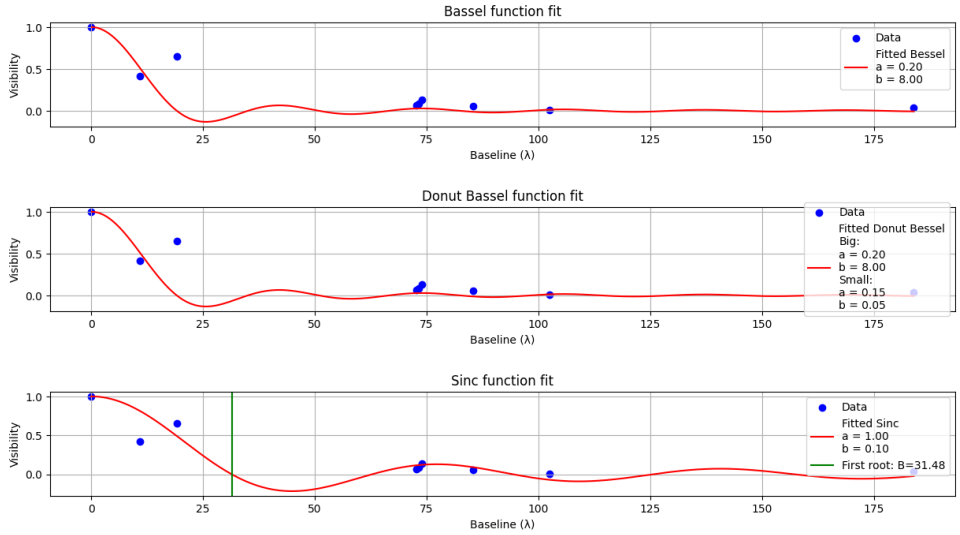

Figure 4.5: The fit of the Bessel, Bessel Donnut, and Sinc function. The green vertical green line in the Sinc plot represents the first root of the Sinc function.

As we can see the fits are not the best due to the lack of data and noise. We evaluated the goodness of fit using the mean absolute error between the fit and the residuals and the results are as follows.

Function	Mean Absolute Error (MAE)
Bessel	0.12
Bessel Donut	0.12
Sinc	**0.09**

Table 4.4: Mean Absolute Error of the fit for the tree different functions.

We can see that the best fit is that of the Sinc function, which suggests that the shape of the radio sun is a square.

The size of the radio sun

The size of the radio sun can be related to the first root of the Sinc function fitted above through,

$$\text{Firts Root} = \frac{\lambda}{\Omega}, \tag{4.5}$$

where Ω is the angular size of the sun. After calculating and converting to the righ units we found that the radio size of the sun is,

$$\Omega = 0.053^\circ \tag{4.6}$$

5 Discussion

In this paper, we successfully demonstrated the process of calibrating and extracting information from an interferometer. We developed a data processing pipeline based on the theoretical framework outlined in Section 2, validating our models for interferometric principles. This included determining visibilities for each baseline, calculating fringe spacing, and ultimately estimating the shape and angular size of the Sun.

However, upon completing the data processing, it became evident that the dataset lacked sufficient data points to enable a reliable function fit for determining the Sun's shape. Additionally, the uneven distribution of data suggested potential interference from atmospheric effects, system noise, or other external factors that contaminated the measurements. Due to limited knowledge of the observational setup, we were unable to fully account for these errors.

One significant discrepancy was the finding that the radio Sun appeared an order of magnitude smaller than expected. While the Sun's typical angular size is approximately 0.5°, our analysis yielded a value of 0.05°. Additionally, we initially anticipated that a Bessel function would provide the best fit, given the Sun's round shape. However, our evaluation using the Mean Absolute Error (MAE) metric indicated that a Sinc function was the best fit, implying a square-shaped Sun—an unexpected result.

While such findings would be groundbreaking under different circumstances, we suspect issues in the later stages of data processing or function fitting led to these anomalies. Further investigation is necessary to identify potential errors and refine our approach to improve the accuracy of our results.

6 Conclusion

In this study, we used the Kapteyn Interferometer for Short-baseline Solar observations (KISS) to analyze the radio Sun's structure and size. We estimated the Sun's angular diameter to be $\Omega = 0.053^\circ$ after finding it's shape to be best described by something apprixamating a square, from the Sinc function fit.

Our findings are missaligned with what we expected due to limitations such as external interference (like for Baseline C), and a very limited number of baseline data. Despite these challenges, the study demonstrates the effectiveness of the data processing and the strength that short-baseline interferometry in solar observations.

Further studies should focus on refining data acquisition techniques, increasing the number of baselines. Enhancing these aspects will provide a more comprehensive understanding of the Sun's radio emission and improve the accuracy of the results.

References

Developers, S. (2025a). *scipy.optimize.curve_fit SciPy v1.11.3 Manual*. Accessed: 2025-01-27.

Developers, S. (2025b). *scipy.signal.find_peaks SciPy v1.11.3 Manual*. Accessed: 2025-01-27.

Jentink, C. (2018). Thesis kiss backend. Master's thesis, University of Groningen. Accessed from https://fse.studenttheses.ub.rug.nl/17874/1/Thesis

Wild, J. P. (1987). The beginnings of radio astronomy in australia. *Publications of the Astronomical Society of Australia*, 7(1):95–102.

A Appendix

Code

All the code used to preprocess the data and estimate the relevant temperatures is available here and is allowed to be viewed duiring grading this report:

https://github.com/Aureusa/Observing-the-Sun-with-KISS

B Appendix

$$\sigma_{P_{max/min}} = \sqrt{\sigma^2_{A_{big/small}} + \sigma^2_{offset_{big/small}}} \tag{B.1}$$

$$\sigma_{P_{avg}} = \sqrt{0.5\sigma^2_{P_{max}} + 0.5\sigma^2_{P_{min}}} \tag{B.2}$$

$$\sigma_{|V(B_\lambda)|} = \sqrt{\left(\frac{2P_{min}}{P_{max}+P_{min}}\sigma_{P_{max}}\right)^2 + \left(\frac{2P_{max}}{P_{max}+P_{min}}\sigma_{P_{min}}\right)^2} \tag{B.3}$$